

Low Dimensional Dynamics of Globally Coupled Complex Riccati Equations: Exact Firing-rate Equations for Spiking Neurons with Clustered Substructure

Diego Pazó¹ and Rok Cestnik²

¹*Instituto de Física de Cantabria (IFCA), Universidad de Cantabria-CSIC, 39005 Santander, Spain*

²*Centre for Mathematical Science, Lund University, 22100 Lund, Sweden*

(Dated: May 21, 2025)

We report on an exact theory for ensembles of globally coupled, heterogeneous complex Riccati equations. A drastic dimensionality reduction to a few ordinary differential equations is achieved for Lorentzian heterogeneity. By applying this technique, we obtain low-dimensional firing-rate equations for populations of spiking neurons with a clustered substructure.

Introduction.— Dimensionality reduction methods are of paramount importance in physics. Keeping only the essential degrees of freedom improves our insight into the system behavior, and increases our chances of controlling it. Standard dimensionality reduction techniques are approximate. Remarkably, years ago, Ott and Antonsen discovered an ansatz which permitted an exact dimensionality reduction to a few ordinary differential equations (ODEs) for populations of heterogeneous phase oscillators [1]. This method was profusely applied to Kuramoto-like models, and pulse-coupled oscillators [2, 3], greatly improving our understanding of them [4]. Subsequently, a close relative of the Ott-Antonsen ansatz, the so-called Lorentzian ansatz, made it possible to derive low-dimensional closed equations for ensembles of spiking neurons of quadratic integrate-and-fire (QIF) type [5]. The Lorentzian ansatz was key for deriving exact firing-rate equations (FREs) [5], i.e. for establishing a theoretical link between ensembles of individual neurons and mesoscopic firing-rate (or neural-mass) dynamics. In subsequent years many variants and extensions of this methodology appeared, see e.g. [6–16]. This framework, known as next-generation neural-mass models [17, 18], was also used in practical and clinical studies in neuroscience [19, 20].

Exact dimensionality reduction appeared to be limited to ensembles of one-dimensional units (phase models or QIF neurons). However, a generalization of the Ott-Antonsen ansatz for orientable agents on a D-dimensional sphere recently appeared [21]. And more recently, one of us found that, like in certain arrays of phase oscillators [22], arrays of *identical* complex-valued Riccati equations are quasi-integrable [23]. Interestingly, the complex Riccati equation, a planar nonlinear system, appears at an intermediate step in the derivation of the FREs mentioned above, as well as in calculations with the Ott-Antonsen ansatz. Therefore, developing a specific dimensionality reduction scheme for ensembles of heterogeneous Riccati equations widens the scope of solvable ensembles in a non-trivial way.

In this Letter we present a dimensionality reduction scheme for ensembles of heterogeneous Riccati equations. The power of this method is exemplified by obtaining exact low-dimensional FREs for ensembles of QIF neurons with a clustered substructure. Numerical simulations confirm the validity of our approach.

Complex-valued Riccati ODEs.— We study ensembles of heterogeneous complex-valued Riccati ODEs:

$$\dot{z}_j = a_j z_j^2 + b_j z_j + c_j, \quad (1)$$

where $z_j(t) \in \mathbb{C}$, and index j runs from 1 to the population size $N \gg 1$. Equation (1) contains three complex coefficients: a_j , b_j , and c_j , which depend on the complex mean field

$$Z(t) = \frac{1}{N} \sum_{j=1}^N z_j. \quad (2)$$

(Explicit dependence on time is also possible.) The coefficients (a_j, b_j, c_j) vary across units, as indicated by the index j . Heterogeneity is introduced via (scalar or vector) parameters η_j , which are drawn from a continuous probability density function (PDF) $G(\eta)$. Hence: $a_j = a(\eta_j, Z, t)$, likewise for b_j and c_j .

Ansatz for the thermodynamic limit.— Our theoretical analysis adopts the thermodynamic limit ($N \rightarrow \infty$). We define a conditional density $\rho(z, \bar{z}|\eta; t)$, which satisfies the continuity equation (expressed with complex variables):

$$\partial_t \rho + \partial_z(\rho \dot{z}) + \partial_{\bar{z}}(\rho \dot{\bar{z}}) = 0, \quad (3)$$

here \bar{z} stands for the complex conjugate of z . We here present the following ansatz as an exact solution of the continuity equation:

$$\rho(z, \bar{z}|\eta; t) = \frac{\alpha(\eta, t)^2}{\pi \left(|z - q(\eta, t)|^2 + \alpha(\eta, t)^2 \right)^2}. \quad (4)$$

This density is bell-shaped, with its center located at $q \in \mathbb{C}$, and radial width $\langle |z - q| \rangle = (\pi/2)\alpha \geq 0$.

The form of (4) was suggested by the stereographic projection of a uniform density on the surface of the unit 3-D sphere onto the complex plane, with an offset q and a width α as free parameters. Originally, the motivation for this stems from the mapping between the dynamics of an orientable agent on a 3-D sphere and the Riccati dynamics with real coefficients, see [24] for illustration.

The functional form of the density (4) is invariant under time evolution, with q and α obeying:

$$\partial_t q(\eta, t) = a q^2 + b q + c - \bar{a} \alpha^2, \quad (5a)$$

$$\partial_t \alpha(\eta, t) = [a q + \bar{a} \bar{q} + (b + \bar{b})/2] \alpha. \quad (5b)$$

Closing this system of equations requires determining the mean field. For a given η value, the average is located at $q(\eta, t)$, and the continuous counterpart of (2) is obtained by integrating q over η :

$$Z(t) = \int G(\eta) q(\eta, t) d\eta \quad (6)$$

Equations (5) and (6) define a closed system of integro-differential equations, which exactly governs the dynamics in the subspace determined by our density ansatz (4).

Reduction to ODEs.— Further reduction to ODEs is possible in certain cases only. We focus hereafter on one of these cases. From now on, only the real part of c_j is heterogeneous:

$$a_j = a(Z, t), \quad (7a)$$

$$b_j = b(Z, t), \quad (7b)$$

$$c_j = \eta_j + i\Gamma + f(Z, t), \quad (7c)$$

where η_j and Γ are real, and $f = f_r + if_i$ is a complex function. Hence, in the $N \rightarrow \infty$ limit, the mean field is obtained by integrating over the only source of heterogeneity:

$$Z(t) = \int_{-\infty}^{\infty} g(\eta) q(\eta, t) d\eta, \quad (8)$$

where $g(\eta)$ is the PDF of η .

A particularly sharp reduction of dimensionality is achieved for a Lorentzian distribution of the heterogeneity, $\eta_j \sim L(\eta_j|\eta_0, \delta)$:

$$g(\eta) = L(\eta|\eta_0, \delta) = \frac{\delta/\pi}{(\eta - \eta_0)^2 + \delta^2}. \quad (9)$$

Here η_0 is the center of the distribution, and $\delta > 0$ denotes its half-width at half-maximum (HWHM). We can evaluate the integral in Eq. (8) using the residue theorem. By closing the integration path with an arc at complex infinity, the integral takes the value of $q(\eta_p, t)$, where η_p is the pole of $g(\eta) = (2\pi i)^{-1}[(\eta - \eta_0 - i\delta)^{-1} - (\eta - \eta_0 + i\delta)^{-1}]$ located inside the integration contour — provided q is analytic inside. The suitable pole turns out to be [25]

$$\eta_p = \eta_0 \pm i\delta, \quad \text{with } \pm = \text{sgn}(\Gamma + f_i - \frac{b_r b_i}{2a}), \quad (10)$$

with $b = b_r + ib_i$, and assuming real $a > 0$. In this way the mean field in Eq. (8) becomes:

$$Z(t) = q(\eta_p, t). \quad (11)$$

Evaluating Eqs. (5) at η_p dramatically reduces the dimensionality of the problem. For closing this system of ODEs we also have to evaluate the variable \bar{q} at the pole η_p . Noting that $\bar{q}(\eta, t)$ is governed by Eq. (5a) under complex conjugation, we end up with a system of three complex-valued ODEs for variables $\{Z, A, Q\} = \{q, \alpha, \bar{q}\}_{\eta=\eta_p}$:

$$\dot{Z} = aZ^2 + bZ + \eta_p + i\Gamma + f - aA^2, \quad (12a)$$

$$\dot{A} = [a(Z + Q) + (b + \bar{b})/2]A, \quad (12b)$$

$$\dot{Q} = aQ^2 + \bar{b}Q + \eta_p - i\Gamma + \bar{f} - aA^2. \quad (12c)$$

This system describes the dynamics of an infinite ensemble of Riccati equations inside the manifold defined by densities of the form in Eq. (4). Next, we showcase the reduced Eqs. (12) on a physically meaningful example.

Firing-rate equations for clustered neurons.— Firing-rate models constitute useful representations of the activity of ensembles of neurons in terms of a few collective variables [18, 26]. A decade ago, an exact reduction to a system of two ODEs was achieved for ensembles of globally coupled QIF neurons [5].

Here we go one step further, and consider a population consisting of N subpopulations of internally coupled QIF neurons. The microscopic equations are:

$$\dot{V}_{i,j} = V_{i,j}^2 + \eta_{i,j} + \phi(r_j) + f(R, t) \quad (13)$$

$$r_j = \frac{1}{M} \sum_{i=1}^M \sum_k \delta^{(\epsilon)}(t - t_{i,j}^k) \quad (14)$$

$$R = \frac{1}{N} \sum_{j=1}^N r_j \quad (15)$$

Here $V_{i,j}(t) \in \mathbb{R}$ is the membrane potential of the i -th neuron, in the j -th subpopulation. The $\delta^{(\epsilon)}$ function in Eq. (14) represents the spikes at firing times $t_{i,j}^k$ (when $V_{i,j}$ reaches ∞ and is reset to $-\infty$), and becomes the Dirac delta after taking $M \rightarrow \infty$. The r_j 's are average firing rates of subpopulations, while R is the global firing rate. The internal coupling in each subpopulation is represented by the function $\phi(r_j)$, while the coupling f in Eq. (13) is the result of every QIF neuron interacting with all the other ones at the global scale.

In the $M \rightarrow \infty$ limit, for Lorentzian distributed internal currents $\eta_{i,j} \sim L(\eta_{i,j}|\eta_j, \Delta)$, applying the method in [5] yields an ensemble of globally coupled FREs. The state of each node is given by the firing rate r_j and the membrane voltage $v_j = M^{-1} \sum_i V_{i,j}$. Their evolution is governed by ODEs:

$$\dot{v}_j = v_j^2 - \pi^2 r_j^2 + \eta_j + \phi(r_j) + f(R, t) \quad (16a)$$

$$\dot{r}_j = 2v_j r_j + \frac{\Delta}{\pi} \quad (16b)$$

Recall that parameters η_j and $\Delta > 0$ are the center and the HWHM of the Lorentzian distribution of internal currents $\eta_{i,j}$ in the j -th subpopulation of QIF neurons [5]. More generally, Δ can represent the sum of the HWHM and the amplitude of Cauchy noise [15, 16]. The main variables and parameters are summarized in Table I.

For physical reasons ϕ has to be a monotonic function with $\phi(0) = 0$. For solvability, we choose the quadratic function $\phi(r) = \kappa r^2$. This is different from the standard linear function, but can be used to approximate a linear interaction around a reference firing rate r_0 : $r \approx r^2/(2r_0) - r_0/2$; or it can appear from triplet interactions. The constant κ represents inhibitory coupling for $\kappa < 0$, and excitatory coupling for $\kappa > 0$.

	Voltages	Rates	Internal Parameters
Neurons	$V_{i,j}$	—	$\eta_{i,j} \sim L(\eta_{i,j} \eta_j, \Delta)$
Subpopulations	v_j	r_j	Δ and $\eta_j \sim L(\eta_j \eta_0, \delta)$
Whole population	V	R	δ and η_0

TABLE I. Variables and internal parameters at each description level for the two examples of dimensionality reduction in this Letter. $L(h|h_0, d)$ indicates h is Lorentzian distributed with center at h_0 and HWHM d . Coupling parameters depend on the specific example and are not included in the Table.

For $\kappa < \pi^2$ we can define the complex variable

$$z_j \equiv v_j + i(\pi^2 - \kappa)^{1/2} r_j, \quad (17)$$

such that Eq. (16) becomes an ensemble of globally coupled Riccati equations:

$$\dot{z}_j = z_j^2 + \eta_j + i(1 - \kappa/\pi^2)^{1/2} \Delta + f(R, t) \quad (18)$$

We adopt the standard chemical coupling $f = JR$, where J is the coupling constant, and $R = \text{Im}(Z)/(\pi^2 - \kappa)^{1/2}$. In Fig. 1 we show the result of simulating an ensemble of 10^4 units with Lorentzian distributed η_j , and an initial condition $z_j(0)$ drawn randomly from the density (4) with η -independent parameters: $q(\eta, 0) = q_0$ and $\alpha(\eta, 0) = \alpha_0$. The two panels in Fig. 1 differ only in the value of α_0 : 0.5 and 2 for (a) and (b), respectively. It may be appreciated that the average Z behaves in very good agreement with the prediction of the corresponding 6-dimensional model (12). The conformity between the simulation and the theory is remarkable, especially considering that the two different initial conditions lead to distinct attractors.

For the system (18), A always approaches zero asymptotically. This follows from the coincidence (up to a factor 6) between the real part of the coefficient accompanying A in Eq. (12b) and the trace of the Jacobian of the system, $6[a\text{Re}(Z + Q) + b_r]$, which determines the volume contraction rate and is negative on average [27] (unless the system is conservative). This means that the asymptotic behaviors of the system are well described by Eq. (12a) alone, setting $A = 0$. One could have derived that equation assuming from the outset that there is a (smooth) univocal dependence of z_j on the value of η_j (i.e., $\alpha = 0$). This assumption enables the transformation $z_j(t) \rightarrow z(\eta, t)$ and immediately leads to Eq. (5a) with $\alpha = 0$.

It is instructive to revert the change of variables defined in (17) and write down the equation for the asymptotic dynamics of mean voltage $V = N^{-1} \sum_j v_j$ and firing rate R :

$$\dot{V} = V^2 - (\pi^2 - \kappa)R^2 + \eta_0 + JR \quad (19a)$$

$$\dot{R} = 2VR + \frac{\Delta}{\pi} + \frac{\delta}{(\pi^2 - \kappa)^{1/2}}. \quad (19b)$$

These two ODEs exactly describe the asymptotic global behavior of an ensemble of QIF neurons with two levels of heterogeneity and coupling. The microscopic level depends on

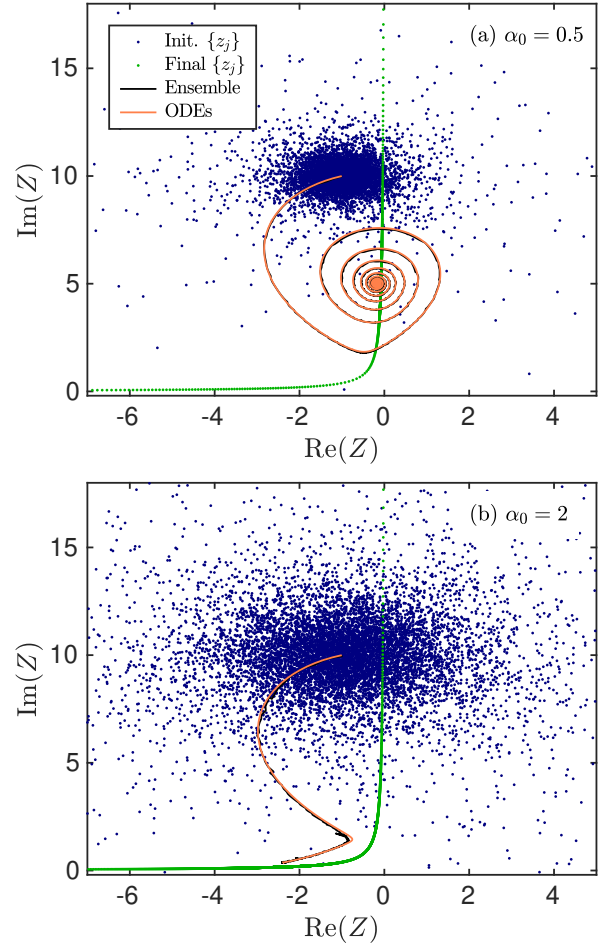


FIG. 1. Phase portraits of the mean field Z for two different initial conditions. The black line is the trajectory of Z obtained by simulating an ensemble of 10^4 units, while the orange line shows the prediction from the reduced model of 3 complex-valued ODEs, Eq. (12). System parameters are: $\kappa = \pi^2/2$, $J = 16$, $\eta_0 = -8$, $\Delta = \delta = 1$. Initial conditions were chosen according to the ansatz (4) with $q_0 = -1 + 10i$, and the only difference between the two panels is the width of the initial distribution α_0 , set to 0.5 in (a) and 2 in (b). The initial and the final state of the ensemble of units $\{z_j\}_{j=1,\dots,N}$ are depicted with blue and green dots, respectively. Animations of the figures are available in the Supplemental Material.

parameters Δ and κ , while at the mesoscopic level δ and J play that role. The phase diagram of system (19) is trivial, since the FRES in [5] are recovered, after appropriate rescaling of R , and defining effective J and Δ parameters. In particular, for $\kappa = 0$ we consistently recover the FRES for Lorentzian heterogeneity of currents centered at η_0 and HWHM $\Delta + \delta$ [28].

Global electrical coupling.— The synapses between neurons can be either chemical or electrical (gap junctions). Electrical coupling may trigger unsteady periodic dynamics in one single population of QIF neurons without additional ingredients such as delay [10]. Hence, we modify our ensemble of QIF neurons considering a global electrical coupling instead

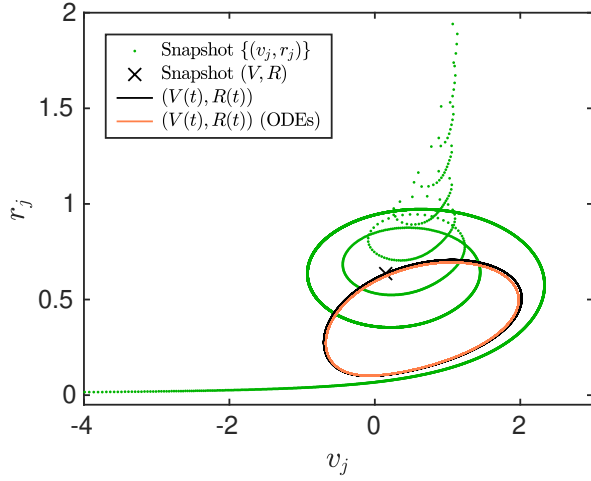


FIG. 2. Snapshot of the coordinates of system (20) with $N = 8000$ in its asymptotic regime, see green dots. The location of the mean field is signaled by a \times . The trajectory of the mean field $(V(t), R(t))$ extracted from the direct simulation of Eq. (20), and the limit cycle predicted by Eq. (21) are depicted by black and orange solid lines, respectively. Parameters: $g = 2.5$, $\kappa = -\pi^2$, $\eta_0 = 1$, and $\Delta = \delta = 0.5$.

of chemical coupling. The form of the internal coupling $\phi(r_j)$ is preserved. The ensemble of FREs turns out to obey [29]:

$$\dot{v}_j = v_j^2 - (\pi^2 - \kappa)r_j^2 + \eta_j + g(V - v_j), \quad (20a)$$

$$\dot{r}_j = 2v_j r_j + \frac{\Delta}{\pi} - g r_j. \quad (20b)$$

Now the global coupling actuates through the mean voltage $V(t)$, and $g > 0$ is the conductance. A global chemical coupling term $J R$ could also be included, but we opted not to do so for simplicity.

We apply transformation (17) and our reduction theory to Eq. (20). If we exclusively focus on the asymptotic dynamics, we need only the complex-valued ODE (12a) with $A = 0$. Written in terms of V and R , it yields exact macroscopic FREs:

$$\dot{V} = V^2 - (\pi^2 - \kappa)R^2 + \eta_0, \quad (21a)$$

$$\dot{R} = 2VR + \frac{\Delta}{\pi} + \frac{\delta}{(\pi^2 - \kappa)^{1/2}} - gR. \quad (21b)$$

We test the validity of these FREs combining global electrical coupling with inhibitory internal coupling ($\kappa < 0$) in each subpopulation. Figure 2 shows the comparison between the oscillatory behavior of the ensemble (20) and the limit cycle displayed by the system of ODEs (21). Again, we find very good agreement between theory and simulation.

Conclusions.— In this work we have uncovered an exact dimensionality reduction scheme for an infinite set of globally coupled complex-valued Riccati equations. Our approach begins with an ansatz for the continuity equation, which defines a lower dimensional manifold. The application of the residue theorem further reduced the dimensionality to only

three complex-valued ODEs, Eq. (12). The mathematical analysis assumed that if an initial $q(\eta, 0)$ possesses an analytic continuation in a particular complex η half-plane, it remains analytic under time evolution. This might not be completely justified since $\bar{q}(\eta, t)$ does not remain analytic in the same half-plane, and it drives q via α . This limitation raises the question of whether the six-dimensional system (12) is merely an excellent approximation. In the large-time limit, $A(t)$ almost always approaches 0, and the resulting asymptotic two-dimensional system exactly describes the attractors (in the thermodynamic limit).

We applied our theory to ensembles of FREs, confirming the validity of our approach. All simulations showed good agreement with the theory. The reduced six-dimensional model consistently predicted the correct asymptotic states across initial conditions, in spite of the analyticity issue discussed above. Moreover, the two-dimensional systems, Eqs. (19) and (21) perfectly described the attractors.

It is noteworthy that with this formalism one could consider arbitrarily nested substructures, since at each step the equations can be of the Riccati form given a certain form of coupling, e.g. for $f = J R^2$, Eq. (19) is equivalent to a Riccati equation [30].

Our methodology represents a significant breakthrough in dimensional reductions as it expands the solvable examples from traditional one-dimensional units into the realm of planar units. This opens up many new examples to explore, with many unit and coupling dynamics one can choose from. Additionally, the heterogeneity may enter in several ways (not only in the real part of c_j). Beyond the variations to the FREs that were studied here, we can also mention the “complexified” Kuramoto model [31, 32] as a system where our methodology can be applied.

DP acknowledges support by Grant No. PID2021-125543NB-I00, funded by MICIU/AEI/10.13039/501100011033 and by ERDF/EU. RC acknowledges financial support from the Royal Swedish Physiographic Society of Lund.

-
- [1] E. Ott and T. M. Antonsen, “Low dimensional behavior of large systems of globally coupled oscillators,” *Chaos* **18**, 037113 (2008).
 - [2] T. B. Luke, E. Barreto, and P. So, “Complete classification of the macroscopic behavior of a heterogeneous network of theta neurons,” *Neural Comput.* **25**, 3207–3234 (2013).
 - [3] D. Pazó and E. Montbrió, “Low-dimensional dynamics of populations of pulse-coupled oscillators,” *Phys. Rev. X* **4**, 011009 (2014).
 - [4] C. Bick, M. Goodfellow, C. R. Laing, and E. A. Martens, “Understanding the dynamics of biological and neural oscillator networks through exact mean-field reductions: a review,” *J. Math. Neurosci.* **10**, 9 (2020).
 - [5] E. Montbrió, D. Pazó, and A. Roxin, “Macroscopic description for networks of spiking neurons,” *Phys. Rev. X* **5**, 021028 (2015).

- [6] D. Pazó and E. Montbrió, “From quasiperiodic partial synchronization to collective chaos in populations of inhibitory neurons with delay,” *Phys. Rev. Lett.* **116**, 238101 (2016).
- [7] I. Ratas and K. Pyragas, “Macroscopic self-oscillations and aging transition in a network of synaptically coupled quadratic integrate-and-fire neurons,” *Phys. Rev. E* **94**, 032215 (2016).
- [8] F. Devalle, A. Roxin, and E. Montbrió, “Firing rate equations require a spike synchrony mechanism to correctly describe fast oscillations in inhibitory networks,” *PLoS Computational Biology* **13**, 1–21 (2017).
- [9] M. di Volo and A. Torcini, “Transition from asynchronous to oscillatory dynamics in balanced spiking networks with instantaneous synapses,” *Phys. Rev. Lett.* **121**, 128301 (2018).
- [10] B. Pietras, F. Devalle, A. Roxin, A. Daffertshofer, and E. Montbrió, “Exact firing rate model reveals the differential effects of chemical versus electrical synapses in spiking networks,” *Phys. Rev. E* **100**, 042412 (2019).
- [11] E. Montbrió and D. Pazó, “Exact mean-field theory explains the dual role of electrical synapses in collective synchronization,” *Phys. Rev. Lett.* **125**, 248101 (2020).
- [12] R. Gast, H. Schmidt, and T. R. Knoesche, “A mean-field description of bursting dynamics in spiking neural networks with short-term adaptation,” *Neural Computation* **32**, 1615–1634 (2020).
- [13] D. S. Goldobin, M. di Volo, and A. Torcini, “Reduction methodology for fluctuation driven population dynamics,” *Phys. Rev. Lett.* **127**, 038301 (2021).
- [14] L. Chen and S. A. Campbell, “Exact mean-field models for spiking neural networks with adaptation,” *Journal of Computational Neuroscience* **50**, 445–469 (2022).
- [15] B. Pietras, R. Cestnik, and A. Pikovsky, “Exact finite-dimensional description for networks of globally coupled spiking neurons,” *Phys. Rev. E* **107**, 024315 (2023).
- [16] P. Clusella and E. Montbrió, “Exact low-dimensional description for fast neural oscillations with low firing rates,” *Phys. Rev. E* **109**, 014229 (2024).
- [17] S. Coombes and Á. Byrne, “Next generation neural mass models,” in *Nonlinear Dynamics in Computational Neuroscience*, edited by F. Corinto and A. Torcini (Springer International Publishing, Cham, 2019) pp. 1–16.
- [18] S. Coombes and K. C. A. Wedgwood, *Neurodynamics: An Applied Mathematics Perspective*, Vol. 75 (Springer Nature, 2023).
- [19] G. Rabuffo, J. Fousek, C. Bernard, and V. Jirsa, “Neuronal cascades shape whole-brain functional dynamics at rest,” *eNeuro* **8** (2021), 10.1523/ENEURO.0283-21.2021.
- [20] M. Gerster, H. Taher, A. Škoch, J. Hlinka, M. Guye, F. Bartolomei, V. Jirsa, A. Zakharova, and S. Olmi, “Patient-specific network connectivity combined with a next generation neural mass model to test clinical hypothesis of seizure propagation,” *Frontiers in Systems Neuroscience* **15**, 675272 (2021).
- [21] S. Chandra, M. Girvan, and E. Ott, “Complexity reduction ansatz for systems of interacting orientable agents: Beyond the Kuramoto model,” *Chaos* **29**, 053107 (2019).
- [22] S. Watanabe and S. H. Strogatz, “Integrability of a globally coupled oscillator array,” *Phys. Rev. Lett.* **70**, 2391–2394 (1993).
- [23] R. Cestnik and E. A. Martens, “Integrability of a globally coupled complex Riccati array: Quadratic integrate-and-fire neurons, phase oscillators, and all in between,” *Phys. Rev. Lett.* **132**, 057201 (2024).
- [24] D. Pazó, “Quasi-integrable arrays: The family grows,” *Physics* **17**, 12 (2024).
- [25] If the sign of $\Gamma + f_i - b_r b_i / (2a)$ changes under the time evolution, then our approach breaks down (one cannot simply flip the sign of the \pm). Fortunately, that does not occur in many situations. See Supplemental Material at xxx for details.
- [26] G. B. Ermentrout and D. H. Terman, *Mathematical foundations of neuroscience*, Vol. 64 (Springer, 2010).
- [27] A. Pikovsky and A. Politi, *Lyapunov Exponents* (Cambridge University Press, Cambridge, UK, 2016).
- [28] This is precisely the marginal distribution for a conditional Lorentzian distribution $L(\eta|\eta_c, \Delta)$ centered at η_c with HWHM Δ , if η_c is itself Lorentzian-distributed with center η_0 and HWHM δ : $\int d\eta_c L(\eta|\eta_c, \Delta) L(\eta_c|\eta_0, \delta) = L(\eta|\eta_0, \delta + \Delta)$.
- [29] The microscopic model of QIF neurons leading to Eq. (20), via [10, 11], is available in the Supplemental Material at XXXX.
- [30] See Supplemental Material at XXX.
- [31] M. Thümler, S. G. M. Srinivas, M. Schröder, and M. Timme, “Synchrony for weak coupling in the complexified Kuramoto model,” *Phys. Rev. Lett.* **130**, 187201 (2023).
- [32] S. Lee, L. Braun, F. Bönisch, M. Schröder, M. Thümler, and M. Timme, “Complexified synchrony,” *Chaos* **34**, 053141 (2024).
- [33] Reversible means that the system remains invariant under time inversion $t \rightarrow -t$ combined with one involution \mathcal{G} (a transformation which applied twice is equal to the identity: $\mathcal{G} \circ \mathcal{G} = 1$). The relevant involution \mathcal{G} is $\beta \rightarrow -\beta - b_r/a$. Each neutral periodic orbits swirls around one of the two neutral foci located on the invariant subspace of the involution $\beta_f = -b_r/(2a)$ —provided $\eta_r > \eta_d = b_r^2/(4a) - f_r + a\alpha^2$.

Supplemental Material to
 “Low Dimensional Dynamics of Globally Coupled Complex Riccati Equations:
 Exact Firing-rate Equations for Spiking Neurons with Clustered Substructure”

SIMULATION DETAILS

Initializing units with prescribed density

We desire initializing units spread according to the density:

$$\rho(z) = \frac{1/\pi}{(|z|^2 + 1)^2} = \frac{1/\pi}{(1 + x^2 + y^2)^2} \quad (\text{S1})$$

We restrict to $q = 0$ and $\alpha = 1$, since the general case just requires a trivial shift and rescaling.

Relation with the uniform density on a sphere

We first note that this density is obtained from a uniform density on the sphere $\tilde{\rho}(\theta, \phi) = (4\pi)^{-1}$ under stereographic projection:

$$x = \frac{\sin \theta \cos \phi}{1 - \cos \theta} \quad ; \quad y = \frac{\sin \theta \sin \phi}{1 - \cos \theta} \quad (\text{S2})$$

Variables θ and ϕ are the polar and azimuthal angles, respectively. We adopt the variable $c \equiv \cos \theta$, such that the differential element of surface $\sin \theta d\theta d\phi$ becomes $dc d\phi$, while $\tilde{\rho}(c, \phi) = (4\pi)^{-1}$. The sought density is found after trivial but convoluted operations following the standard transformation:

$$\rho(x, y) = \tilde{\rho}(c, \phi) \left| \frac{\partial(c, \phi)}{\partial(x, y)} \right| \quad (\text{S3})$$

As mentioned, the density (S1) is the result of projecting a uniform density on the sphere. Random drawing from the distribution (S1) is performed taking θ and ϕ at random and apply the transformation in (S2). While ϕ is uniformly sampled in the interval $[0, 2\pi)$, some care must be taken with θ . The differential $dc \equiv d \cos \theta$ dictates we have to take a random quantity w in the interval $[-1, 1]$ and obtain the polar angle as $\theta = \arccos w$.

Initialization (alternative)

Working in polar coordinates $z = r e^{i\varphi}$, we can take φ at random. For the radius note that the radial density reads

$$p(r) = \frac{2}{(1 + r^2)^2} \quad (\text{S4})$$

The cumulative distribution function is

$$P(r) = \int_0^r p(r') r' dr' = \frac{r^2}{1 + r^2} \quad (\text{S5})$$

Sampling a uniform random variable w in the unit interval, we get $r = \sqrt{w/(1-w)}$.

Sampling of η_j

The values of the $\{\eta_j\}_{j=1, \dots, N}$ were selected deterministically using quantiles of the Lorentzian distribution:

$$\eta_j = \eta_0 + \delta \tan[(\pi/2)(2j - N - 1)/(N + 1)] \quad (\text{S6})$$

Numerical integration

For the simulation of the ensemble of Riccati equations we used a Runge-Kutta integrator with adaptive stepsize control. The nominal stepsize was in the range $10^{-3} - 10^{-4}$.

CALCULATION OF THE MEAN FIELD

We calculate the mean field replacing the integral along the real axis by a contour integration \oint defined closing the real line by an arc at infinity (either in the upper or in the lower half-plane $\eta = |\eta|e^{i\theta} \in \mathbb{C}$):

$$Z = \int_{-\infty}^{\infty} g(\eta) q(\eta, t) d\eta = \oint g(\eta) q(\eta, t) d\eta - \lim_{|\eta| \rightarrow \infty} i|\eta| \int_0^{\pm\pi} g(\eta) q(\eta, t) e^{i\theta} d\theta = q(\eta_p, t) \quad (\text{S7})$$

The last equality is true if:

1. The only pole ($\eta_p = \eta_0 \pm i\delta$) inside the integration contour comes from the Lorentzian distribution

$$g(\eta) = \frac{\delta/\pi}{(\eta - \eta_0)^2 + \delta^2} = \frac{1}{2\pi i} \left[\frac{1}{\eta - \eta_0 - i\delta} - \frac{1}{\eta - \eta_0 + i\delta} \right]. \quad (\text{S8})$$

We analyze below in which half-plane is q analytic, i.e. if $q(\eta, 0)$ is initially analytic it remains so.

2. The integration along the arc vanishes.

Analytic continuation

The application of the residue theorem requires q to possess an analytic continuation from the real η to complex $\eta = \eta_r + i\eta_i$ in one half-plane ($\eta_i > 0$ or $\eta_i < 0$).

We write the equation for $q = \beta + i\gamma$ in real variable:

$$\partial_t \beta = a(\beta^2 - \gamma^2) + b_r \beta - b_i \gamma + \eta_r + f_r - a\alpha^2 \quad (\text{S9a})$$

$$\partial_t \gamma = 2a\beta\gamma + b_r \gamma + b_i \beta + \eta_i + \Gamma + f_i \quad (\text{S9b})$$

It is not obvious at first sight how the time evolution of q , governed by these equations, could break the analyticity of a certain analytic initial condition $q(\eta, 0)$. We gain insight assuming constant α and f . The key observation is that at

$$\eta_i = -\Gamma - f_i + \frac{b_r b_i}{2a} \quad (\text{S10})$$

the system in Eq. (S9) is reversible. This is relevant on the half-line $\eta_r \in (\eta_d, \infty)$, since it exhibits a continuum of periodic orbits[33]. In turn, there is a discontinuity in $q(\eta, t)$ when crossing this half-line (S10) in the complex η -plane. This is something we avoid choosing the opposite half-plane when applying the residue theorem in Eq. (S7).

Vanishing integral along the arc

We analyze next the behavior of q in the large $|\eta|$ limit. The governing equations become:

$$\partial_t \beta = \beta^2 - \gamma^2 + |\eta| \cos \theta \quad (\text{S11a})$$

$$\partial_t \gamma = 2\beta\gamma + |\eta| \sin \theta \quad (\text{S11b})$$

As we wish to know the behavior of the system at $|\eta| \rightarrow \infty$ the linear and finite terms have been neglected. It is easy to ascertain that there is a stable fixed point at $(\beta_*, \gamma_*) = (\tilde{\beta}, \tilde{\gamma})|\eta|^{1/2}$, with $\tilde{\beta}, \tilde{\gamma} \sim O(1)$ and $\tilde{\beta} < 0$. This immediately implies that the integration along the arc in Eq. (S7) vanishes since $g(\eta) \sim |\eta|^{-2}$

DERIVATION OF THE ENSEMBLE OF FIRING-RATE EQUATIONS FROM SPIKING NEURONS

The microscopic model consists of N subpopulations of M QIF neurons each. Each neuron is identified by two indices i and j , indicating the neuron number and population number, respectively. A neuron receives inputs from its own subpopulation (through the firing rate r_j), as well as a global input from all neurons.

Global chemical coupling

We start with the system of QIF neurons in Eqs. (13)-(15).

The heterogeneity in each subpopulation is Lorentzian with half-width at half-maximum (HWHM) Δ . The center $\bar{\eta}_j$ is itself Lorentzian distributed:

$$h(\eta_{i,j}|\bar{\eta}_j) = \frac{\Delta/\pi}{(\eta_{i,j} - \bar{\eta}_j)^2 + \Delta^2} \quad (\text{S12})$$

$$g(\bar{\eta}_j) = \frac{\delta/\pi}{(\bar{\eta}_j - \eta_0)^2 + \delta^2} \quad (\text{S13})$$

In the thermodynamic limit, the system of equations (13), (14), (S12) reduces, via the theory developed in [5], to the ensemble of firing-rate models, Eq. (16) in the main text. There, $\bar{\eta}_j$ has been replaced by η_j to lighten the notation.

Note that the distribution of $\eta_{i,j}$ among all the population is a Lorentzian centered at η_0 with HWHM $\Delta + \delta$:

$$\int_{-\infty}^{\infty} h(\eta|\bar{\eta})g(\bar{\eta})d\bar{\eta} = \frac{(\Delta + \delta)/\pi}{(\eta - \eta_0)^2 + (\Delta + \delta)^2}$$

Global electrical coupling

The system of equations is:

$$\dot{V}_{i,j} = V_{i,j}^2 + \eta_{i,j} + \phi(r_j) + g(V - V_{i,j}) \quad (\text{S14})$$

$$v_j = \frac{1}{M} \sum_{i=1}^M V_{i,j} \quad (\text{S15})$$

$$V = \frac{1}{N} \sum_{j=1}^N v_j \quad (\text{S16})$$

Using the theory developed in [5, 10] with symmetric spikes [11] we get:

$$\dot{v}_j = v_j^2 - \pi^2 r_j^2 + \phi(r_j) + \eta_j + g(V - v_j) \quad (\text{S17a})$$

$$\dot{r}_j = 2v_j r_j + \frac{\Delta}{\pi} - g r_j \quad (\text{S17b})$$

For $\phi(r) = \kappa r^2$, and the transformation $z_j = v_j + i(\pi^2 - \kappa)^{1/2} r_j$, the ensemble of Riccati equations becomes:

$$\dot{z}_j = z_j^2 - g z_j + \eta_j + i(1 - \kappa/\pi^2)^{1/2} \Delta + gV \quad (\text{S18})$$

With our reduction method we get:

$$\dot{Z} = Z^2 - g Z + \eta_0 + i \left[(1 - \kappa/\pi^2)^{1/2} \Delta + \delta \right] + gV \quad (\text{S19})$$

Recalling that $Z = V + i(\pi^2 - \kappa)^{1/2} R$ we get the macroscopic rate equations (21) in the main text.

SEVERAL LAYERS OF NETWORKS AND HETEROGENEITY

In the main text, we study an ensemble of ensembles of QIF neurons. This effectively creates a two-layer system —i.e., a network of networks. This approach can be extended to systems with multiple scales. In this section, we present the formulation for a three-layer system: micro, meso, and macro.

At the micro level, we consider individual QIF neurons, indexed by three variables: i , j , and k , representing the micro, meso, and macro levels, respectively. Thus, variable V_{ijk} denotes the voltage of a neuron in the macro population “ k ”, within the meso population “ j ”, and with the microscopic index “ i ”.

The QIF equation for every neuron is given by:

$$\dot{V}_{ijk} = V_{ijk}^2 + \phi_0(r_{jk}) + \phi_1(r_k) + \phi_2(R) + \eta_{ijk} \quad (\text{S20})$$

Here, ϕ_0 , ϕ_1 , and ϕ_2 represent the coupling terms at the micro, meso, and macro scales, respectively. The term r_{jk} represents the firing rate of the meso-macro population labeled by “ jk ”, r_k is the firing rate of the macro population “ k ”, and R denotes the global firing rate. These are defined as follows:

$$r_{jk} = \frac{1}{N_0} \sum_{i=1}^{N_0} \sum_{\ell} \frac{1}{\tau} \int_{t-\tau}^t \delta(s - t_{ijk}^{\ell}) ds, \quad r_k = \frac{1}{N_1} \sum_{j=1}^{N_1} r_{jk}, \quad R = \frac{1}{N_2} \sum_{k=1}^{N_2} r_k \quad (\text{S21})$$

where t_{ijk}^{ℓ} is the time of the ℓ^{th} spike of neuron “ ijk ”, and we consider the infinite limit $N_0, N_1, N_2 \rightarrow \infty$ and $\tau \rightarrow 0$. Similarly, the mean voltages at each level are expressed as:

$$v_{jk} = \frac{1}{N_0} \sum_{i=1}^{N_0} V_{ijk}, \quad v_k = \frac{1}{N_1} \sum_{j=1}^{N_1} v_{jk}, \quad V = \frac{1}{N_2} \sum_{k=1}^{N_2} v_k \quad (\text{S22})$$

The heterogeneity $\eta_{ijk} \in \mathbb{R}$ follows a Lorentzian distribution at all levels:

$$g_0(\eta_{ijk}) = \frac{\Delta_0/\pi}{(\eta_{ijk} - \eta_{jk})^2 + \Delta_0^2}, \quad g_1(\eta_{jk}) = \frac{\Delta_1/\pi}{(\eta_{jk} - \eta_k)^2 + \Delta_1^2}, \quad g_2(\eta_k) = \frac{\Delta_2/\pi}{(\eta_k - \eta)^2 + \Delta_2^2} \quad (\text{S23})$$

where parameters Δ_0 , Δ_1 , and Δ_2 control the width of the Lorentzian distributions at the micro, meso, and macro scales, respectively.

Layer 1: Meso-Scale Dynamics via Lorentzian Ansatz

We now apply the Lorentzian ansatz formalism [5] to the voltage equation (S20) to describe the dynamics at the meso scale. The resulting equation is:

$$\dot{z}_{jk} = z_{jk}^2 + \phi_0 + \phi_1 + \phi_2 + \eta_{jk} + i\Delta_0 \quad (\text{S24})$$

Here, the complex variable z_{jk} represents both the mean voltage and firing rate, with $z_{jk} = v_{jk} + i\pi r_{jk}$. By expressing the dynamics in terms of real quantities, we obtain:

$$\dot{v}_{jk} = v_{jk}^2 - \pi^2 r_{jk}^2 + \phi_0 + \phi_1 + \phi_2 + \eta_{jk} \quad (\text{S25a})$$

$$\dot{r}_{jk} = 2v_{jk}r_{jk} + \frac{\Delta_0}{\pi} \quad (\text{S25b})$$

Now we choose the coupling at the micro level to be $\phi_0(r_{jk}) = \kappa_0 r_{jk}^2$ and change the dynamic variables with a transformation:

$$q_{jk} = v_{jk} + ir_{jk}\sqrt{\pi^2 - \kappa_0} \quad (\text{S26})$$

Under this transformation, we obtain a new system of coupled Riccati equations for the variables q_{jk} :

$$\dot{q}_{jk} = q_{jk}^2 + \phi_1 + \phi_2 + i\Delta_0\sqrt{1 - \kappa_0/\pi} + \eta_{jk} \quad (\text{S27})$$

Layer 2: Macro-Scale Dynamics

Now that the Riccati array (S27) is complex, we employ the formalism detailed in the main text. Moving to the next scale, we describe the dynamics as follows:

$$\dot{q}_k = q_k^2 + \phi_1 + \phi_2 + i\Delta_0\sqrt{1 - \kappa_0/\pi} + i\Delta_1\eta_k \quad (\text{S28})$$

It is important to note that q_k is not simply the complex voltage variable for this scale, i.e. $q_k \neq v_k + i\pi r_k$. Instead we have to consider the inverse transformation (S26), and write the mean voltage and firing rate equation at the macro scale:

$$\dot{v}_k = v_k^2 - (\pi^2 - \kappa_0)r_k^2 + \phi_1 + \phi_2 + \eta_k \quad (\text{S29a})$$

$$\dot{r}_k = 2v_k r_k + \frac{\Delta_0}{\pi} + \frac{\Delta_1}{\sqrt{\pi^2 - \kappa_0}} \quad (\text{S29b})$$

These equations are analogous to those derived in the main text, see Eqs. (19).

Now in order to get a Riccati array again, we choose the coupling at the meso level to be $\phi_1(r_k) = \kappa_1 r_k^2$ and change the dynamic variables with another transformation:

$$w_k = v_k + i r_k \sqrt{\pi^2 - \kappa_0 - \kappa_1} \quad (\text{S30})$$

and obtain yet another system of coupled Riccati equations for the variables w_k :

$$\dot{w}_k = w_k^2 + \phi_2 + i\Delta_0\sqrt{1 - \kappa_0/\pi^2 - \kappa_1/\pi^2} + i\Delta_1\sqrt{1 - \frac{\kappa_1}{\pi^2 - \kappa_0}} + \eta_k \quad (\text{S31})$$

Layer 3: Global Dynamics

Following the approach from the previous subsection, we again apply the our ansatz to describe the dynamics at the global level. The evolution of the global variable is given by:

$$\dot{w} = w^2 + \phi_2 + i\Delta_0\sqrt{1 - \kappa_0/\pi^2 - \kappa_1/\pi^2} + i\Delta_1\sqrt{1 - \frac{\kappa_1}{\pi^2 - \kappa_0}} + i\Delta_2 + \eta \quad (\text{S32})$$

which relates to the global mean voltage V and the global firing rate R via the expression: $w = V + iR\sqrt{\pi^2 - \kappa_0 - \kappa_1}$. The corresponding dynamics for v and r are:

$$\dot{V} = V^2 - (\pi^2 - \kappa_0 - \kappa_1)R^2 + \phi_2 + \eta \quad (\text{S33a})$$

$$\dot{R} = 2VR + \frac{\Delta_0}{\pi} + \frac{\Delta_1}{\sqrt{\pi^2 - \kappa_0}} + \frac{\Delta_2}{\sqrt{\pi^2 - \kappa_0 - \kappa_1}} \quad (\text{S33b})$$

These equations describe the global behavior of the system in terms of the firing rate and mean voltage, incorporating the couplings and heterogeneities across all three scales.

Generalization to arbitrary number of scales

At this point the pattern is visible: for $M + 1$ layers, the global firing rate and voltage equations are:

$$\dot{V} = V^2 - (\pi^2 - \kappa_0 - \kappa_1 - \dots - \kappa_{M-1})R^2 + \phi_M + \eta \quad (\text{S34a})$$

$$\dot{R} = 2VR + \frac{\Delta_0}{\pi} + \frac{\Delta_1}{\sqrt{\pi^2 - \kappa_0}} + \frac{\Delta_2}{\sqrt{\pi^2 - \kappa_0 - \kappa_1}} + \dots + \frac{\Delta_M}{\sqrt{\pi^2 - \kappa_0 - \kappa_1 - \dots - \kappa_{M-1}}} \quad (\text{S34b})$$
